AMERICAN SOCIETY FOR MICROBIOLOGY | Microbiology Spectrum

| Vaccines | Research Article

Intranasal SARS-CoV-2 RBD decorated nanoparticle vaccine enhances viral clearance in the Syrian hamster model

Devanshi R. Patel,[1,2] Allen M. Minns,[2,3,4] Derek G. Sim,[2,5] Cassandra J. Field,[1,2] Abigail E. Kerr,[1,2] Talia A. Heinly,[1,2] Erin H. Luley,[1,6] Randall M. Rossi,[2] Carol M. Bator,[2] Ibrahim M. Moustafa,[3] Elizabeth B. Norton,[7] Susan L. Hafenstein,[2,3,8] Scott E. Lindner,[2,3,4] Troy C. Sutton[1,2]

AUTHOR AFFILIATIONS See affiliation list on p. 17.

ABSTRACT Multiple vaccines have been developed and licensed for severe acute respiratory syndrome coronavirus-2 (SARS-CoV-2). While these vaccines reduce disease severity, they do not prevent infection. To prevent infection and limit transmission, vaccines must be developed that induce immunity in the respiratory tract. Therefore, we performed proof-of-principle studies with an intranasal nanoparticle vaccine against SARS-CoV-2. The vaccine candidate consisted of the self-assembling 60-subunit I3-01 protein scaffold covalently decorated with the SARS-CoV-2 receptor-binding domain (RBD) using the SpyCatcher-SpyTag system. We verified the intended antigen display features by reconstructing the I3-01 scaffold to 3.4 A using cryogenicelectron microscopy. Using this RBD-grafted SpyCage scaffold (RBD + SpyCage), we performed two intranasal vaccination studies in the "gold-standard" pre-clinical Syrian hamster model. The initial study focused on assessing the immunogenicity of RBD + SpyCage combined with the LTA1 intranasal adjuvant. These studies showed RBD + SpyCage vaccination induced an antibody response that promoted viral clearance but did not prevent infection. Inclusion of the LTA1 adjuvant enhanced the magnitude of the antibody response but did not enhance protection. Thus, in an expanded study, in the absence of an intranasal adjuvant, we evaluated if covalent bonding of RBD to the scaffold was required to induce an antibody response. Covalent grafting of RBD was required for the vaccine to be immunogenic, and animals vaccinated with RBD + SpyCage more rapidly cleared SARS-CoV-2 from both the upper and lower respiratory tract. These findings demonstrate the intranasal SpyCage vaccine platform can induce protection against SARS-CoV-2 and, with additional modifications to improve immunogenicity, is a versatile platform for the development of intranasal vaccines targeting respiratory pathogens.

IMPORTANCE Despite the availability of efficacious COVID vaccines that reduce disease severity, SARS-CoV-2 continues to spread. To limit SARS-CoV-2 transmission, the next generation of vaccines must induce immunity in the mucosa of the upper respiratory tract. Therefore, we performed proof-of-principle, intranasal vaccination studies with a recombinant protein nanoparticle scaffold, SpyCage, decorated with the RBD of the S protein (SpyCage + RBD). We show that SpyCage + RBD was immunogenic and enhanced SARS-CoV-2 clearance from the nose and lungs of Syrian hamsters. Moreover, covalent grafting of the RBD to the scaffold was required to induce an immune response when given via the intranasal route. These proof-of-concept findings indicate that with further enhancements to immunogenicity (e.g., adjuvant incorporation and antigen optimization), the SpyCage scaffold has potential as a versatile, intranasal vaccine platform for respiratory pathogens.

KEYWORDS vaccines, SARS-CoV-2, hamster

Editor Rafael A. Medina, Emory University School of Medicine, Atlanta, Georgia, USA

Address correspondence to Scott E. Lindner, Scott.Lindner@psu.edu, or Troy C. Sutton, tcs38@psu.edu.

We wish to disclose the following intellectual property claims related to this study: Lindner, S.E. & Hafenstein, S. US Patent Application 16/494,502 "Versatile Display for Proteins"; Lindner, S.E., Hafenstein, S., & Butler, N. PCT/US2020/033785 "Specific Selection of Immune Cells Using Versatile Display Scaffolds"; Lindner, S.E., Sutton, T.C., Hafenstein, S., & Butler, N. US Trademark Application 9063755

See the funding table on p. 17.

Received 5 December 2022
Accepted 17 January 2024
Published 9 February 2024

Severe acute respiratory syndrome coronavirus-2 (SARS-CoV-2) is the etiological agent of the coronavirus disease 2019 pandemic (1). SARS-CoV-2 is an enveloped betacoronavirus with a non-segmented positive-sense single-stranded RNA genome. The genome encodes four structural proteins: spike (S), membrane (M), envelope (E), and nucleocapsid (N), as well as multiple non-structural proteins (2). The S protein is the major surface protein and mediates viral entry and fusion. The receptor-binding domain (RBD) of the S protein binds the host receptor angiotensin-converting enzyme 2 (ACE2), leading to endocytosis of the virion and infection of the host (2, 3). Importantly, antibody responses against SARS-CoV-2 in humans and experimentally infected animals are predominantly directed toward the S protein. Moreover, titers of RBD-binding antibodies correlate with neutralizing activity, and RBD is considered the immunodominant region of the S protein (4, 5). Therefore, RBD represents a suitable immunogen for vaccine development, and blocking this domain has the potential to prevent infection.

Prior to the SARS-CoV-2 pandemic, vaccines targeting coronaviruses in humans had not been advanced through late-stage clinical trials. Development of multiple SARS-CoV-2 vaccine candidates was enabled by rapid sequencing of the viral genome as well as pre-existing knowledge about vaccination against severe acute respiratory syndrome coronavirus and Middle Eastern respiratory syndrome coronavirus (6). Currently, there are at least 12 vaccines approved for human use (7, 8). Licensed vaccines such as CoronaVac and QazCovid-in contain inactivated virus (9–13), while vaccines developed by Pfizer/BioNTech and Moderna consist of mRNA encoding the pre-fusion S protein enclosed in a lipid nanoparticle (14). The Novavax vaccine contains recombinant S protein, and vaccines from Johnson & Johnson and AstraZeneca use viral vectors to deliver DNA encoding the S protein (15). Importantly, all of these licensed vaccines are delivered by intramuscular (i.m.) injection, and these vaccines have been shown to reduce the severity of SARS-CoV-2 infection (11, 16, 17); however, these vaccines do not prevent infection, and vaccinated individuals can develop symptomatic infections and transmit the virus onward.

Intramuscular vaccination induces a systemic immune response with high titers of IgG antibodies that enter the lungs to reduce viral replication and disease severity (6, 18). However, the delivery of vaccines via the i.m. route does not induce a strong mucosal immune response (6), and a mucosal response is required to prevent infection of the upper respiratory tract and limit transmission. Indeed, both our research group and others have shown that inducing mucosal and systemic immunity by prior SARS-CoV-2 infection can protect against infection and severe disease (19–23). In contrast to i.m. administered vaccines, an efficacious intranasal vaccine has the potential to protect mucosal surfaces via the induction of secretory IgA antibodies and mucosal T cells. Moreover, these vaccines can also induce a serum IgG response that can impart similar disease reductions as observed for existing vaccines [reviewed in reference (24)]. However, ongoing analyses of licensed SARS-CoV-2 vaccine efficacy have shown that vaccine-induced immunity wanes over time, resulting in breakthrough infections (25–27). In addition, intranasal administration of mRNA vaccines to mice did not confer protection against SARS-CoV-2 challenge (28). As a result, there is a growing need to develop a second generation of SARS-CoV-2 vaccines that can be administered through theintranasal route to induce protective mucosal immunity (29, 30).

To date, a limited number of intranasal vaccine candidates have been developed against SARS-CoV-2. Most of these candidates are viral vectors or live-attenuated vaccines; however, there have been safety concerns with viral vectored SARS-CoV-2 vaccines, and their administration is limited to individuals older than 18 years of age (31, 32). Moreover, the only licensed live-attenuated intranasal vaccine is against influenza, and due to safety concerns and poor immunogenicity in older individuals, its use is restricted to individuals 2–49 years of age (33). Therefore, there is a need to develop intranasal vaccines that would be suitable for individuals of all ages.

To address this gap, we adapted the I3-01 self-assembling protein into a nanoparticle bearing a flexible SpyCatcher domain (SpyCage) to display SARS-CoV-2 RBD/SpyTag (RBD

+ SpyCage) as an intranasal vaccine. The I3-01-based platform has been shown to be an excellent immunization scaffold to present a variety of antigens from viral (SARS-CoV-2, influenza, Epstein-Barr Virus, and Classical swine fever virus) and parasitic (*Plasmodium*) pathogens that reproducibly boosts immune responses as compared to the unscaffolded antigen (34–41). However, these trials have been restricted to i.m. injections with immune responses as endpoint readouts, with a few notable studies proceeding through challenges with live pathogens (40, 42).

Here, we performed proof-of-principle studies to evaluate RBD grafted to the SpyCage scaffold (RBD +SpyCage) as an intranasal vaccine in the "gold-standard" Syrian hamster model. Syrian hamsters are highly permissive to SARS-CoV-2 infection, and the virus efficiently transmits in these animals by direct contact and respiratory droplets (i.e., airborne transmission) (19–21). We performed two separate efficacy studies in which hamsters were given a prime and boost intranasal vaccination and challenged with SARS-CoV-2. In the initial study, we assessed vaccine efficacy when the LTA1 intranasal adjuvant was included with the vaccine candidate. LTA1 is a well-characterized intranasal adjuvant derived from heat-labile (LT) *Escherichia coli* enterotoxin. LTA1 is the enzymatic A1 domain of this protein but lacks the B-subunit, which alters cellular binding and prevents cranial nerve toxicity. In pre-clinical studies, incorporation of LTA1 into intranasal vaccines against inactivated influenza, tetanus toxoid, and *Klebsiella pneumoniae* protein antigens enhanced immunogenicity and protective efficacy of the vaccines (43–46). In a follow-up study, we demonstrated that covalent grafting of RBD to SpyCage was required to induce an IgG antibody response in vaccinated animals. Upon SARS-CoV-2 challenge, regardless of vaccination status, all hamsters became infected and exhibited weight loss; however, animals vaccinated with RBD + SpyCage more rapidly cleared the virus from both the upper and lower respiratory tracts with evidence of reduced lung pathology. Collectively, these studies demonstrate the potential for SpyCage as the basis of an intranasal vaccine platform for SARS-CoV-2 and possibly other respiratory pathogens.

MATERIALS AND METHODS

Production and purification of apo cage and SpyCage

The apo cage scaffold is based upon the 6xHis/I3-01 protein described previously by Hsia and colleagues (47, 48). The SpyCage scaffold consists of a genetic fusion of a 6xHis tag, the SpyCatcher domain, a flexible linker, and the I3-01 protein (47, 49). These proteins were expressed in the *E. coli* BL21 (DE3) CodonPlus strain bearing either plasmid pSL1013 (apo cage) or pSL1040 (SpyCage) using a modified pET28 vector. Cultures were grown in LB media at 37°C to an OD600 of ~0.5, at which point protein expression was induced by the addition of 0.5-mM IPTG (final concentration) for 2.5 hours. Cell pellets were suspended in 50 mL of resuspension buffer [50-mM Tris-Cl, pH 8.0, at room temperature (RT), and 500-mM NaCl] per 1 L of culture, and cells were lysed by sonication using a disruptor horn attachment, using three pulses of 30 s each at 70% amplitude and 50% duty cycle (model 450 Branson Digital Sonifier). The crude extract was spun at 15,500 × *g* for 20 minutes at 4°C, and the soluble fraction was then incubated in batch with 2 mL of equilibrated Ni-NTA resin for 1 hour at 4°C. The resin was applied to a gravity flow column and washed with 50 mL of resuspension buffer followed by 50 mL of mid-imidazole buffer (25-mM Tris-Cl, pH 7.5, at RT, 500-mM NaCl, 50-mM imidazole, 250-mM dextrose, and 10% vol/vol glycerol). Apo cage and SpyCage protein were eluted using elution buffer (50-mM Tris-Cl, pH 8.0, at RT, 500-mM NaCl, and 300-mM imidazole) and then exhaustively dialyzed into 50-mM Tris-Cl, pH 8.0, at RT, 500-mM NaCl, 1-mM dithiothreitol (DTT), and 10% vol/vol glycerol. The dialyzed material was then concentrated to ~2.0 mg/mL using Amicon Ultra Centrifugal Filters (Thermo Fisher Scientific, Cat #UFC9-003-08) and snap-frozen in liquid nitrogen for long-term storage at −80°C. Complete plasmid sequences are provided in File S1.

Production and purification of SARS-CoV-2 spike RBD

The RBD of SARS-CoV2-2 spike protein was produced with and without a C-terminal SpyTag for covalent attachment to SpyCage using plasmid pSL1515 and pSL1510, respectively (49). Plasmid DNA was purified (Qiagen HiSpeed Maxiprep Kit), precipitated with ethanol, and resuspended in water before transfection using the Expi293 Expression System (Thermo Fisher Scientific; Expi293F cells, Expi293 Media, and the ExpiFectamine 293 Transfection Kit) by the Penn State Sartorius Cell Culture Facility as per manufacturer instructions. Briefly, cells maintained in log-phase growth at 37°C and 8% CO_2 in baffled flasks, shaking at 120–130 rpm, were transfected at a concentration of 5 × 10^6 /mL and supplemented by the addition of ExpiFectamine 293 Transfection Enhancer 1 and 2 approximately 20 hours post-transfection. Culture supernatant was harvested by centrifugation (274 × *g*, 5 minutes, RT) on day 3 and was incubated in batch with Ni-NTA (Thermo Scientific HisPur) resin pre-equilibrated in 1× phosphate-buffered saline (PBS) at 4°C for 1 hour on a nutator. The resin was then applied to a gravity flow column and was washed four times with 10-column volumes of wash buffer (57-mM NaH_2PO_4, pH 6.3, at RT, 30-mM NaCl, and 20-mM imidazole). Protein was eluted with four-column volumes of elution buffer (57-mM NaH_2PO_4, pH 7.9, at RT, 30-mM NaCl, and 235-mM imidazole). Eluted protein was dialyzed to completion in 1× PBS and snap-frozen in liquid nitrogen for long-term storage at −80°C. Complete plasmid sequences are provided in File S1.

Covalent bonding of SARS-CoV-2 spike RBD to SpyCage

Purified SpyCage was dialyzed into 1× PBS with 1-mM DTT and then mixed with purified SARS-CoV-2 spike RBD + SpyTag or with RBD only at a 1.2:1 molar ratio of RBD to SpyCage monomer in a buffer consisting of 1× PBS and 1-mM DTT. The binding reaction was allowed to go to completion by incubation for 3 hours at RT. The extent of SpyCage saturation was assessed by SDS-PAGE as previously described (49). The binding reaction was then dialyzed into 1× PBS and stored at −80°C until use in immunization efforts.

Cryo-EM specimen preparation and data collection

Purified apo cage protein complex based on I3-01 (47, 48) was first assessed by negative staining to check sample quality and concentration before preparing transmission electron microscopy (TEM) grids for data collection. Briefly, a 3.5-µL aliquot was applied to a glow-discharged Cu grid coated with a thin film of continuous carbon, washed, stained with 0.75% wt/vol uranyl formate for 15 s, blotted, air-dried, and loaded on EFI Tecnai G2 Spirit BioTwin microscope (120 kV) for imaging.

TEM grids (QUANTAFOIL R2/1; QUANTAFOIL, Germany) were plasma cleaned using a PELCO Glow Discharge System (Ted Pella, Redding, CA). Aliquots of 3.5 µL of the apo cage sample at approximately 0.1 mg/mL were applied to the grids, blotted for 2 s, and then plunge-frozen in liquid ethane using a vitrification robot (Vitrobot, Thermo Fisher Scientific). Grids were stored in liquid nitrogen until the date of screening and data collection. Data were acquired on a Thermo Fisher Titan Krios electron microscope (300 kV) equipped with a Falcon 3EC direct detection camera. EPU software (v.2.13.0.3175REL) was used to set up data acquisition at a nominal magnification of ×59,000 and a physical pixel size of 1.11 Å/pixel. A total of 1,220 micrographs were recorded as movies (stacks of 39 frames) at an exposure rate of 1.15 e/Å^2/frame and a total exposure time of 69.8 s. The nominal defocus range of −1.2 to −3.0 µm was applied during data collection.

Cryo-EM image processing

Image analysis was performed using cryoSPARC software package (v.3.3.2) (50). Aligned movie stacks were generated from raw micrographs after correcting for stage drift and anisotropic motion using patch motion correction. Parameters of the contrast transfer function (CTF) were estimated for each aligned movie in patch mode. Manually selected 283 particles from 11 micrographs were used to train a Topaz model for particle picking; a box of 420 × 420 pixel size was used for particle extraction (51). The trained model was

applied to pick 129,792 particles from 1,202 micrographs. Further cleaning of the data using two-dimensional (2D) classification resulted in 63,430 particles for subsequent data processing. A map from an *ab initio* model (generated using 10,000 particles), along with the selected clean particles, was subjected to homogenous refinement in cryoSPARC. Local motion correction (52) of the refined particles followed by homogenous refinement with higher-order CTF terms enabled (including beam-tilt, spherical aberration, trefoil, and tetrafoil) and icosahedral symmetry (I1) enforced resulted in a final map at 3.4-Å resolution.

Cryo-EM model building

The initial model of the apo cage monomer was extracted from the published I3-01 model (47, 48). The monomer model was manually fitted into the 3.4-Å map in ChimeraX (53); a full icosahedral model of apo cage was generated from the asymmetric unit. PHENIX real-space refinement was used to refine the model against the sharpened map with non-crystallographic symmetry parameters applied (54). The refined model was visually inspected in Coot and validated by MolProbity (55, 56). All figures of the protein structure and cryo-electron microscopy (EM) map were created using ChimeraX.

Culture of SARS-CoV-2

The SARS-CoV-2/USA/WA1/2020 isolate was received from The World Reference Center for Emerging Viruses and Arboviruses, University of Texas Medical Branch at Galveston. The virus was obtained at passage 4 and was subcultured once on Vero E6/TMPRSS2 cells (Japanese Collection of Research Bioresources Cell Bank). All titrations of virus stocks and tissue homogenates were performed on Vero E6 cells (American Type Culture Collection) cultured in Dulbecco's modified Eagle Medium (DMEM) (Cytiva) supplemented with 10% fetal bovine serum (FBS), 4-mM L-glutamine, 1-mM sodium pyruvate (Corning), 1× non-essential amino acids, and 1× antibiotic and antimycotic (Corning) at 37°C with 5% CO_2. For culture of the VeroE6/TMPRSS2 cells, 1-mg/mL geneticin was added to the media, and the FBS was reduced to 5%. To determine the titer of viral stocks, the tissue culture infectious dose 50% ($TCID_{50}$) was determined by inoculating cells grown in 24-well plates with serial dilutions of the virus. The plates were incubated at 37°C with 5% CO_2 and scored for cytopathic effect at 96 hours post-infection (p.i.). The $TCID_{50}$ was then calculated using the method of Reed and Muench (57).

Vaccination and challenge experiments

Equal numbers of male and female, 6- to 8-week-old Syrian hamsters (HsdHan:AURA; Envigo, Haslett, MI) were used for all studies. After acclimatization, the animals were implanted with a subcutaneous transponder chip (Bio Medic Data Systems), and a pre-vaccination blood sample was collected. For intranasal vaccination and virus inoculation, the animals were sedated and intranasally inoculated with a vaccine candidate (70 µL in 1× PBS) or SARS-CoV-2 (100 µL in DMEM). For all experimental procedures, hamsters were sedated with 150-mg/kg ketamine, 7.5-mg/kg xylazine, and 0.015-mg/kg atropine via intraperitoneal injection. After completion of the procedure, hamsters were given 1-mg/kg atipamezole subcutaneously. For tissue collection and at the end of each study, hamsters were humanely euthanized via CO_2 asphyxiation.

Trial 1: evaluation of immunogenicity and efficacy of the SpyCage-RBD vaccine candidate

To evaluate the immunogenicity and efficacy of the SpyCage RBD vaccine, groups of hamsters (n = 14/group) were intranasally vaccinated with PBS (mock), SpyCage (15 µg), SARS-CoV-2 RBD (10 µg), LTA1 (10 µg), SARS-CoV-2 RBD (10 µg) bound to SpyCage (15 µg, "RBD + SpyCage"), or SARS-CoV-2 RBD (10 µg) bound to SpyCage (15 µg, RBD + SpyCage) + LTA1 (10 µg). Animals received a primary (1°) vaccination and a secondary (2°) vaccination 28 days later. LTA1 adjuvant was provided by Dr. Elizabeth Norton (Tulane

University) and was prepared as previously described (45, 46). Blood samples were collected via gingival vein from six animals (three males and three females) per group on days 14, 26, 42, and 55 post-1° vaccination. Blood samples were centrifuged at 1,000 × *g* for 10 minutes at RT, and serum was collected and stored at −20°C. On day 56 post-1° vaccination (i.e., 28 days post-2° vaccination), all animals were intranasally inoculated with 10^5 $TCID_{50}$ SARS-CoV-2/USA/WA1/2020. On days 3 and 6 post-infection (day 59 and 62 post-1° vaccination), lung and nasal turbinate tissues were collected (*n* = 4/group, 2 males and 2 females) and stored at −80°C. The remaining six hamsters were monitored for weight loss until day 14 (day 70 post-primary vaccination).

Trial 2: assessment of the requirement for grafting of RBD to SpyCage

Groups of hamsters (*n* = 18/group) were intranasally vaccinated with PBS (mock), SpyCage (15 µg), SARS-CoV-2 RBD (10 µg), SARS-CoV-2 RBD without SpyTag (10 µg) mixed with SpyCage (15 µg) (i.e., RBD could not covalently bond to SpyCage, "RBD| SpyCage"), and SARS-CoV-2 RBD (10 µg) grafted to SpyCage (15 µg, RBD + SpyCage). These vaccines were formulated without LTA1 adjuvant. The vaccination and blood collection protocols were the same as in the initial study, and on day 56 post-1° vaccination, animals were challenged with 1,000 $TCID_{50}$ of SARS-CoV-2. On days 3, 5, and 7 post-challenge (days 59, 61, and 63 post-primary vaccination), lung and nasal turbinates were collected [*n* = 4/group (2 males and 2 females)]. One lung lobe was fixed with 10% vol/vol normal buffered formalin, and the remaining lung lobes and nasal turbinates were stored at −80°C. The remaining six hamsters/group were monitored for weight loss until day 14 post-SARS-CoV-2 challenge (day 70 post-primary vaccination). All animals were euthanized on day 15 post-SARS-CoV-2 challenge.

Viral titration of tissue samples

Collected lungs and nasal turbinates were homogenized in 2% FBS-DMEM containing 2× antibiotic and antimycotic using an Omni tissue homogenizer. The homogenates were centrifuged at 1,000 × *g* for 10 minutes at 4°C, and the supernatant was titrated to determine the $TCID_{50}$ on Vero E6 cells as previously described (58).

Microneutralization assay

To determine titers of neutralizing antibodies, microneutralization assays were performed on Vero E6 cells as previously described (59).

ELISA

To assess the levels of RBD-binding IgG and IgA antibodies, enzyme-linked immunosorbent assays (ELISA) was performed according to a protocol generously provided by Dr. Sabra Klein, Johns Hopkins, School of Public Health (23, 60).

Histopathology

Formalin-fixed lung samples were processed and stained with hematoxylin and eosin as previously described (23). Slides were scored by a board-certified veterinary pathologist using established methods (61). Each animal was scored for the extent of lesions (0–4), alveolar damage (0–3), bronchial damage (0–3), blood vessel damage (0–3), hemorrhage (0–2), and type II pneumocyte hyperplasia (0–2). For each animal, a total pathology score was obtained by calculating the sum of scores.

Biocontainment and animal care and use

All experiments using SARS-CoV-2 were conducted in an animal biosafety Level 3 enhanced laboratory. This facility is approved by the US Department of Agriculture and the Centers for Disease Control and Prevention.

Statistical analysis

Prism GraphPad (v.9.0) was used to perform all statistical analyses with $P < 0.05$ considered significant. Weight loss and viral titers at each time point were evaluated for normality by D'Agostino and Pearson test. For data sets that passed the normality test, one-way analysis of variance with post hoc Tukey's test was performed. When data sets did not pass the normality test, Kruskal-Wallis tests with a post hoc Dunn's multiple comparison test were performed. Histopathological scores were also compared using non-parametric Kruskal-Wallis tests with a post-hoc Dunn's multiple comparison.

RESULTS

Cryo-EM reconstruction and refinement of an atomic model of the apo cage scaffold

To establish a robust, multimeric, spherical protein-based scaffold for intranasal immunizations that would mimic the size of a viral particle, we selected a wireframe dodecahedron based upon the previously described I3-01 protein, which was designed to self-assemble from 60 monomers (47, 48). To validate this scaffold structurally, we assessed a purified sample of this apo cage complex by electron microscopy. Samples were first quality controlled by negative staining with uranyl formate to assess particle integrity and concentration, and were then vitrified on gold grids for cryo-EM data collection on our home-source Titan Krios electron microscope equipped with a Falcon 3EC direct detection camera. Data processing and all aspects of the cryo-EM workflow were conducted in cryoSPARC software (v.3.3.2) (50).

To create an experimentally determined high-resolution model, we collected a cryo-EM data set with 1,220 recorded movies to yield 1,202 processed micrographs with good-quality ice. These were used to auto-pick and extract 129,792 particles using a box size of 420 × 420 pixels (calibrated pixel size = 1.11 Å) (Fig. 1A; Table S1). Then 2D classification was used to clean up the data by removing junk particles (Fig. 1B) to produce a total of 63,430 particles for cryo-EM map reconstruction and refinement while imposing icosahedral symmetry. The refinement produced a cryo-EM map at an average resolution of 3.4 Å and an estimated local resolution in the range of 3.0–5.0 Å (Fig. 1C). Map resolution was determined based on the gold-standard criterion that applies a Fourier shell correlation cutoff value of 0.143 (Fig. 1D) (62). The 3.4-Å resolution map showed the typical features of the designed apo cage with an average diameter of 25 nm and the trimeric protein units occupying the vertices of the pentameric faces of the dodecahedron. The I3-01 design PDB of this protein structure was modified and used to initiate model building (47, 48). The map density was clear enough to build the atomic structure using the published model of I3-01 to provide the starting coordinates. Real-space refinement of the icosahedral model in PHENIX resulted in a 3.4-Å resolution model (Fig. 1E) with a cross-correlation value for model vs vmap of 0.77 (CC masked, Table S1). The geometrical parameters of the refined model checked by MolProbity revealed a good quality model with a MolProbity score of 1.5, with approximately 98% of residues in the favored region and no residues in the disallowed region of the Ramachandran plot. Quality-check parameters of the model and map-model agreement are listed in Table S1. The 3.4-Å resolution map showed clear density for most side chains of the amino acids constituting the apo cage protein (aa 22–222) (Fig. 1F). However, as expected for structures solved in the range of 3- to 4-Å resolution (63), directionality of some carbonyl groups could not be resolved unambiguously.

Comparing the solved cryo-EM structure and that from the computationally designed I3-01 model (47, 48) showed that the two structures are almost identical (root mean square values of 0.57 Å for 200 Cα atoms and 1.29 Å for all non-hydrogen atoms), but the side chain atoms of surface residues had minor differences between our experimental and the computationally designed structures.

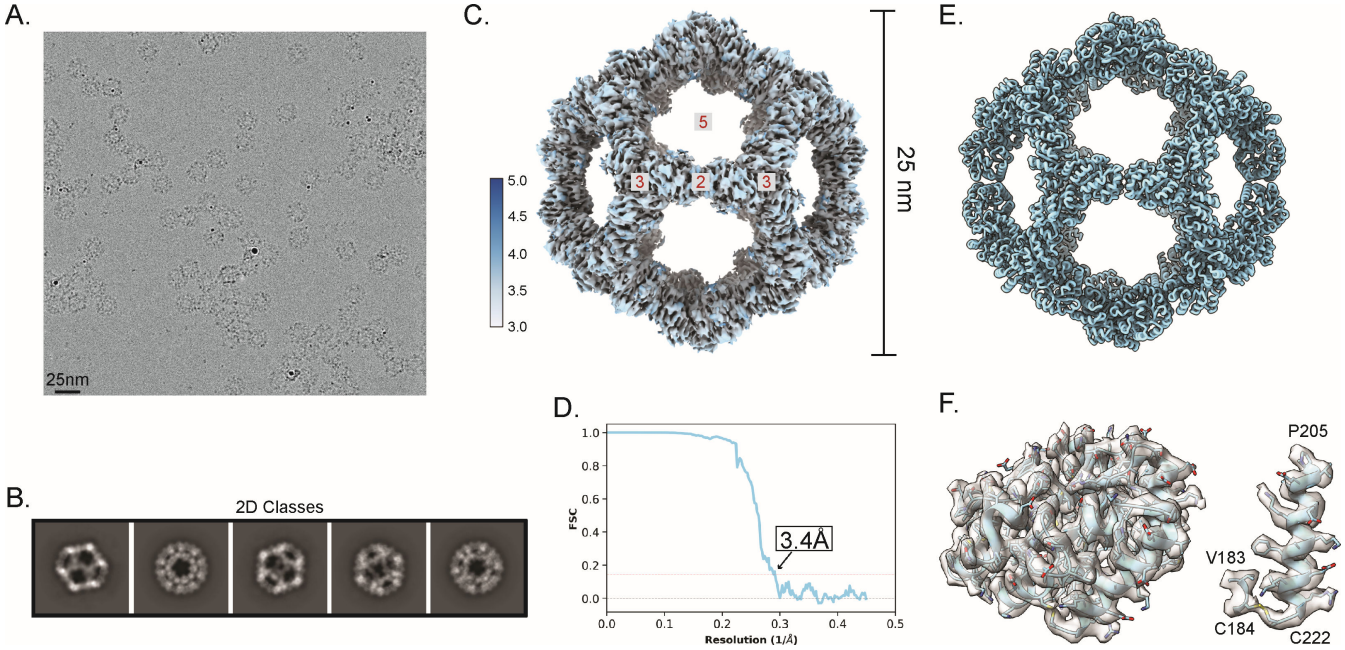

FIG 1 Single-particle analysis and cryo-EM reconstruction of the apo cage used for immunizations. (A) A representative cryo-EM micrograph of apo cage particles (scale bar, 25 nm) is provided. (B) Examples of representative class averages from a 2D classification of the particles extracted from cryo-EM micrographs are provided. (C) A reconstructed icosahedral map of the apo cage structure is colored according to the estimated local resolution; color key is shown to the left of the map. Red numbers in gray boxes on the structural model indicate the two-, three- and fivefold symmetry axes of the dodecahedron. Apo cage particles have an approximate diameter of 25 nm. (D) A Fourier shell correlation (FSC) curve of the reconstructed map using gold-standard refinement in cryoSPARC is presented. An approximate map resolution of 3.4 Å based on 0.143 FSC cutoff is indicated. (E) An atomic model of the apo cage was built by applying icosahedral symmetry in ChimeraX to an asymmetric unit fitted to the density of the map shown in panel C. (F) (Left) A portion of the map covering a single I3-01 monomer is rendered as a transparent surface, with the fitted model (aa 22–222) shown as a light blue cartoon with side chains represented as sticks. (Right) A close-up view of residues Val183 and Cys184 and the C-terminal helix (aa 205–222) showing clear density of the assigned side chains is shown with the map contoured at level 0.9 in ChimeraX. The quality of density is sufficient to observe the disulfide bond between Cys184 and the C-terminal Cys222.

Covalent bonding of SARS-CoV-2 spike RBD to SpyCage

As the wireframe cage scaffold was robust, spherical, symmetrical, and could outwardly present up to 60 fused proteins of interest, we selected it for further modification for antigen display. Because the genetic fusion of antigens directly to protein-based scaffolds can influence expression levels, solubility, and purification conditions needed, we leveraged the SpyTag/SpyCatcher system to covalently link antigens of interest to the scaffold following its purification (49). This approach enables substantial versatility to load different proteins and their variants without modifying the scaffold itself and has been used for a variety of viral and parasitic pathogens to enhance immune responses (34–36, 39–41, 64). To this end, we appended a SpyCatcher domain with a flexible linker to the N-terminus of I3-01 so that all 60 subunits bear this capture domain (schematic in Fig. 2A). We observed that this self-assembling scaffold fused with SpyCatcher capture domains displayed excellent solubility and stability profiles when expressed in *E. coli*, as it expressed to high levels and did not precipitate in standard laboratory conditions (Fig. 2B). A comparable arrangement has been described for the mi3 variant of I3-01, which also exhibited favorable display properties (35). This scaffold, which we have termed SpyCage, was advanced for all immunization studies presented here.

The use of SpyTag/SpyCatcher elements permits the versatile loading of antigens that are independently expressed in an ideal expression system for that protein, thus ensuring that proper post-translational modifications and processing events occur. Here, using 293F suspension cells, we produced the RBD of SARS-CoV-2 Spike protein with a C-terminal 6xHis tag, and either with or without an additional C-terminal SpyTag (Fig.

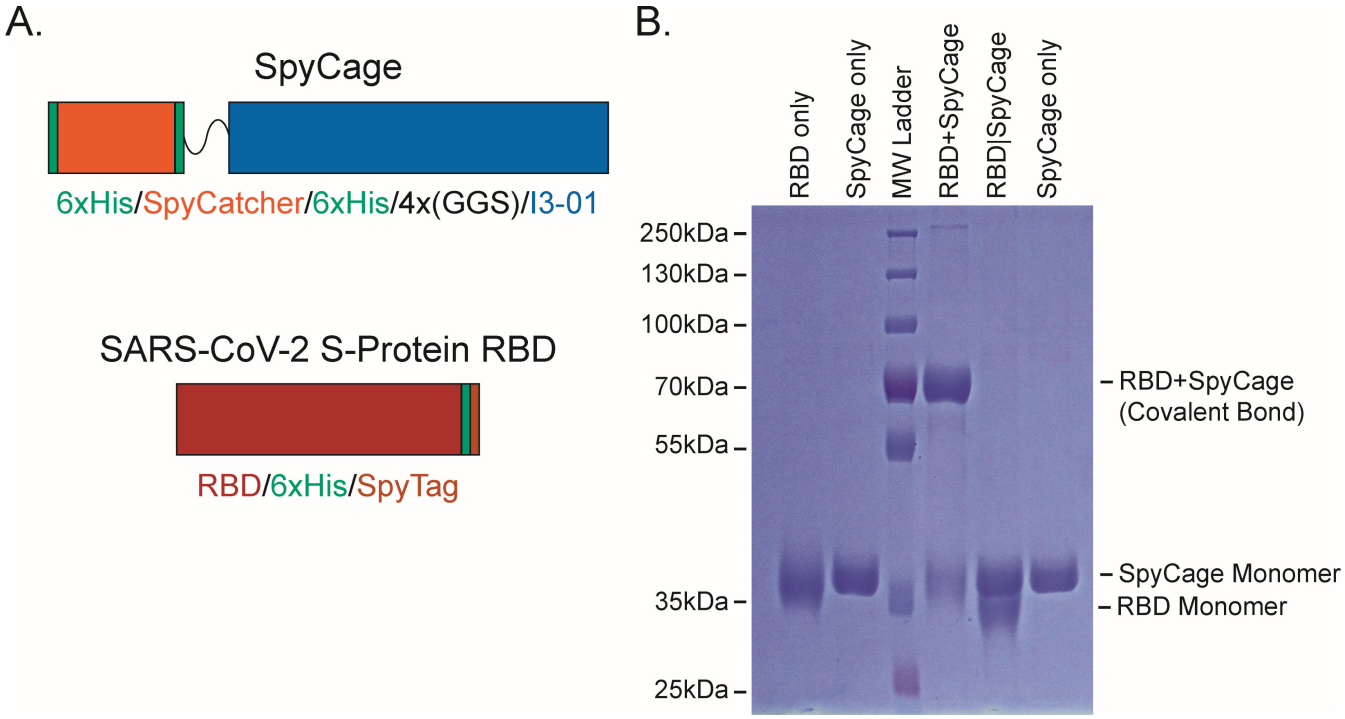

FIG 2 Display of RBD via the SpyCage scaffold. (A) A schematic of the SpyCage scaffold illustrates 6xHis purification tags, the SpyCatcher capture domain, a flexible linker, and a C-terminal I3-01 variant used to create the self-assembling protein wireframe platform. A schematic of RBD with a C-terminal 6xHis tag and with/without a C-terminal SpyTag is shown. (B) SDS-PAGE of SpyCage, RBD, SpyCage + RBD, and SpyCage|RBD preparations. The covalent bonding ("grafting") of RBD to SpyCage is evident when RBD bears a SpyTag, but not in its absence as per a mobility shift. SpyCage approaches saturation with RBD at a 1.0-to-1.2 molar ratio of SpyCage-to-RBD, as has been seen with other antigens of comparable shape and mass.

2A). Secreted protein was purified from the culture supernatant to >99% purity via Ni-NTA affinity chromatography (Fig. 2B). Mixing of SpyCage with RBD (RBD + SpyCage) at a 1.0-to-1.2 molar ratio in 1× PBS led to the formation of a covalent bond that could be detected by a mobility shift by SDS-PAGE with >95% saturation of the scaffold with RBD (Fig. 2B). This molar ratio consistently achieves this maximal degree of saturation for RBD and other comparably sized, globular antigens (data not shown). In contrast, when SpyCage was mixed with RBD lacking a SpyTag (RBD|SpyCage), no covalent linkage formed between the RBD and SpyCage, as intended (Fig. 2B). This second combination creates an admixture (RBD|SpyCage) that permits testing of the effect that covalent bonding of the antigen to the scaffold has upon efficacy. From this, we conclude that SpyCage is a stable and saturable antigen display platform capable of presenting antigens of interest in a versatile mix-and-go format. As SpyCage has similar structural properties to a virus particle and displays 5–15 copies of an antigen on a single face of the scaffold (up to a total of 60 antigens per particle), we hypothesized SpyCage grafted with RBD would be a greatly improved vaccine candidate. As there is an urgent need for the development of vaccines inducing mucosal immunity, we proceeded to evaluate SpyCage as an intranasal vaccine.

RBD grafting to SpyCage is required to induce an antibody response

To assess the immunogenicity of RBD + SpyCage as an intranasal vaccine candidate (i.e., trial 1), hamsters were given a 1° and 2° intranasal vaccine consisting of PBS (mock), SpyCage, LTA1, RBD, RBD + SpyCage, or RBD + SpyCage + LTA1. The two vaccine doses were administered 28 days apart, and serum samples were collected prior to each vaccination and the day before viral challenge. To assess the antibody response, levels of RBD-binding IgG antibodies in the serum were quantified by ELISA, and neutralizing

antibodies were assayed by a microneutralization assay. We found that only the RBD + SpyCage and RBD + SpyCage + LTA1 vaccinated animals developed an IgG antibody response (Fig. S1A). On day 28, one of six and four of six animals in the RBD + SpyCage and RBD + SpyCage + LTA1 groups had IgG antibodies against RBD, respectively. The proportion of animals that developed an antibody response increased on day 55. At this time point, four of six animals given RBD + SpyCage, and six of six animals given RBD + SpyCage + LTA1 developed an antibody response (Fig. S1A). However, while these antibodies were able to bind RBD, they exhibited minimal neutralizing activity (Fig. S1B). In the RBD + SpyCage group, none of the animals developed a neutralizing antibody response, while in the RBD + SpyCage + LTA1 animals, three of six animals developed low titers (<1:25) of neutralizing antibodies.

Subsequently, we conducted a modified vaccine study (designated trial 2) to determine if grafting of RBD directly to SpyCage through covalent bonding was required to induce an antibody response. Animals were vaccinated according to the same regimen; however, the LTA1 adjuvant groups were excluded because the adjuvant did not enhance efficacy in trial 1 (see results below). Instead, an additional group in which RBD without SpyTag was mixed with SpyCage (RBD|SpyCage) was included to test the importance of the covalent bonding of RBD to SpyCage. Therefore, the experimental groups consisted of animals given the following vaccines: (i) mock (PBS), (ii) RBD, (iii) SpyCage, (iv) RBD mixed with but not bound to SpyCage (RBD|SpyCage), and (v) RBD grafted to SpyCage (RBD + SpyCage). In both vaccination studies, animals were monitored for 7 days post-1° and 2° vaccination for adverse effects. None of the animals exhibited weight loss or clinical signs, indicating the vaccine was well tolerated (data not shown).

Evaluation of the antibody response by ELISA and microneutralization assay (Fig. 3) showed that none of the mock, SpyCage, RBD alone, or RBD|SpyCage immunized animals developed RBD-directed antibodies on day 28 or 55. In contrast, animals vaccinated with RBD + SpyCage developed IgG antibodies against RBD on day 28 post-1° vaccination (two of six animals positive) and on day 55 (five of six animals positive) (Fig. 3A). While most animals in the RBD + SpyCage group developed IgG antibodies by day 55, only one animal developed an IgA antibody response (Fig. 3B). This was one of the two animals that developed IgG antibodies early (day 28) and was the animal with the highest IgG antibody titer on day 55 (1:12,800) (Fig. 3A). In addition, the serum from this animal exhibited neutralizing activity (Fig. 3C), while none of the other animals developed a neutralizing antibody response. Thus, while we did not observe 100% seroconversion, the RBD + SpyCage vaccine candidate was reproducibly capable of inducing IgG antibodies. As one animal developed both a neutralizing antibody response and IgA antibodies indicative of mucosal immunity, our findings indicate that, with additional modifications to enhance immunogenicity, intranasal vaccination with RBD + SpyCage could induce mucosal immunity. Furthermore, these findings demonstrate the RBD + SpyCage vaccine provides a substantial boost in antibody responses compared to RBD alone or an RBD|SpyCage admixture where the covalent bond needed for grafting cannot form.

To address the immunogenicity of SpyCage itself, we also evaluated the antibody response to SpyCage by ELISA (Fig. 3D). All animals given a vaccine containing SpyCage developed IgG antibodies directed toward the scaffold. While there were no statistically significant differences between different vaccine groups that received the SpyCage, the RBD|SpyCage admixture increased the antibody response twofold compared to animals given SpyCage alone, and RBD + SpyCage further increased the response by twofold (i.e., fourfold relative to SpyCage alone). These findings indicate that grafting the antigen to SpyCage enhances the antibody response to both the scaffold and the antigen.

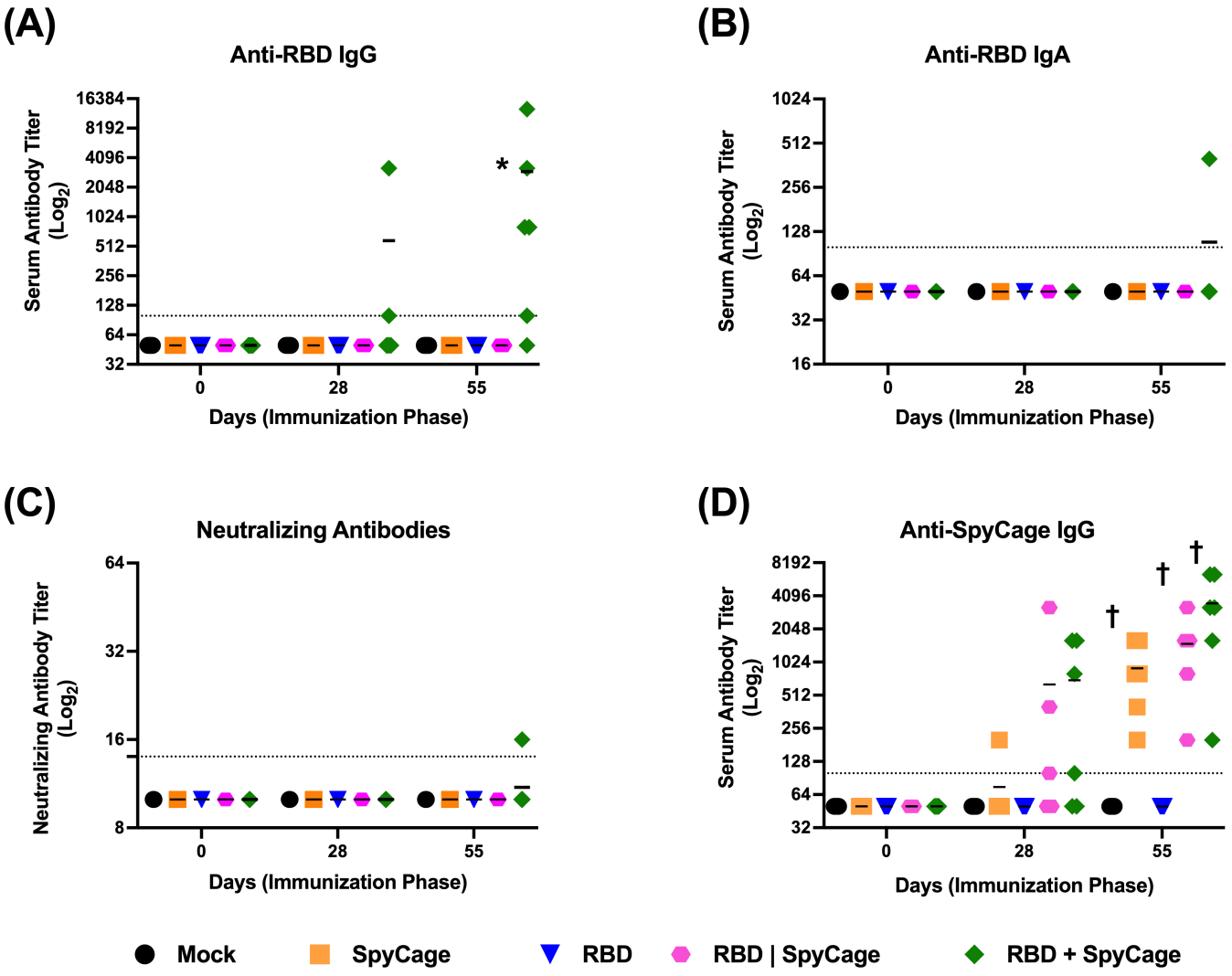

FIG 3 Binding and neutralizing antibody responses to intranasal vaccination with RBD + SpyCage. Antibody titers were measured in serum samples on days 0, 28, and 55, prior to primary vaccination, boost vaccination, and viral challenge, respectively. Plotted are (A) anti-RBD IgG, (B) IgA titers, (C) neutralizing antibody titers against SARS-CoV-2, and (D) IgG antibody titers against the SpyCage scaffold. *Significantly different from all other groups by Kruskal-Wallis with Dunn's multiple comparison; †significantly different from mock and RBD groups.

Intranasal vaccination with RBD + SpyCage enhances clearance of SARS-CoV-2 from the respiratory tract

To assess the efficacy of the RBD + SpyCage vaccine candidate in both vaccine trials of this study, we assessed whether RBD + SpyCage enhanced viral clearance and reduced clinical illness. In the second trial, we also evaluated the effect of vaccination on reducing lung pathology. In trial 1, which included animals that received the vaccine formulated with LTA1 adjuvant, vaccinated hamsters were challenged with 10^5 $TCID_{50}$ SARS-CoV-2 on day 56 post-1° vaccination (day 28 post-2° vaccination). After viral challenge, animals were monitored for weight loss for 14 days, and on days 3 and 5 p.i., lung and nasal turbinate samples were collected from a subset of animals (n = 4/group/time point) (Fig. S2). After viral challenge, animals in all experimental groups lost weight (Fig. S2A), and there were no statistically significant differences between the groups; however, the animals that received RBD + SpyCage had reduced weight loss, and by the end of the study, these animals exceeded their pre-challenge weight. When we evaluated viral titers in the lungs and nasal turbinates, on day 3 p.i. all experimental groups had high titers of replicating virus in these tissues with no significant differences between groups. On day

6 p.i., viral titers in both tissues were reduced for all groups; however, while a proporation of mock, SpyCage, LTA1, and RBD + LTA1 vaccinated animals had replicating virus in the nose and lungs, no replicating virus was recovered from the RBD only and RBD + SpyCage vaccinated animals (Fig. S2B and C). Unfortunately, for the group that received the RBD + SpyCage + LTA1, the day 6 animals had to be removed from the study prior to viral challenge due to veterinary concerns unrelated to vaccination. However, these findings suggested vaccination with RBD or RBD + SpyCage facilitated viral clearance.

While vaccination with either RBD only or RBD + SpyCage reduced viral load on day 6, only the RBD + SpyCage or RBD + SpyCage + LTA1 vaccinated animals developed an IgG antibody response. We therefore performed a second, expanded vaccination study (i.e., trial 2) to evaluate if grafting of RBD to SpyCage via covalent bonding was required for protection. Here, we repeated the vaccination study with an additional group of animals that were vaccinated with an admixture of RBD and SpyCage where the covalent bond needed for grafting could not form (RBD|SpyCage). As the LTA1 adjuvant did not reduce weight loss or viral titers beyond antigen alone, we did not use the LTA1 adjuvant in these studies. Moreover, as the 10^5 $TCID_{50}$ challenge dose used in the initial study is two to three orders of magnitude higher than the estimated infectious dose for humans (i.e., 100–1,000 infectious units) (65, 66), we reduced the challenge dose to 1,000 $TCID_{50}$ of SARS-CoV-2. This challenge dose was previously shown to induce weight loss in hamsters (21), which we also verified with our virus stock (Fig. S3). Finally, to evaluate the dynamics of viral clearance more comprehensively, we modified the time points of tissue collection such that tissues were collected on days 3, 5, and 7 p.i.

After viral challenge, the animals in all experimental groups lost weight, with peak weight loss at day 6 or 7. However, while there were no statistically significant differences in weight loss between experimental groups (Fig. 4A), consistent with our first study, we also observed that animals vaccinated with RBD + SpyCage trended toward reduced weight loss compared to the other groups (Fig. 4A). We next evaluated viral replication in the nasal turbinates and lungs. On day 3 p.i., mean viral load in the nasal turbinates and lungs for all groups were comparable, with titers greater than 10^5 and 10^6 $TCID_{50}$/g in each tissue, respectively (Fig. 4B and C). However, on day 5 p.i., the mean viral titer in the nasal turbinates for the RBD + SpyCage group was significantly lower (25 $TCID_{50}$/g) compared to the other experimental groups (titer range: 881–3,955 $TCID_{50}$/g) (Fig. 4B). Similarly, in the lungs, RBD + SpyCage vaccinated animals also had significantly lower titers (1,183 $TCID_{50}$/g) (titer range for other experimental groups: 11,988–59,356 $TCID_{50}$/g) (Fig. 4C). On day 7 p.i., replicating virus was not detected in the nasal turbinates or lungs from any of the experimental groups (Fig. 4B and C). Therefore,

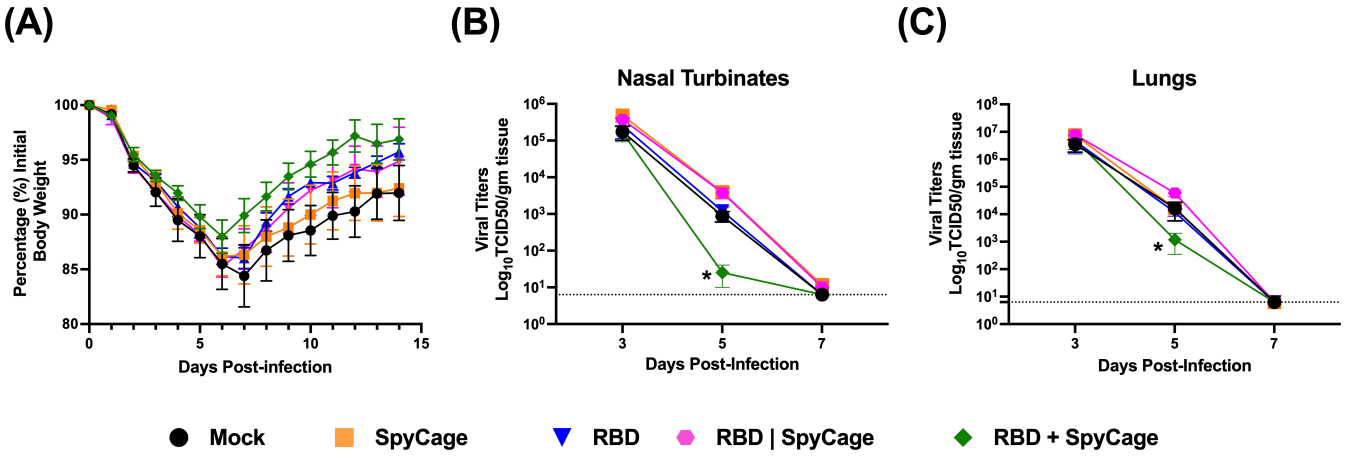

FIG 4 Weight loss and viral titers in the nasal turbinates and lungs after SARS-CoV-2 challenge of vaccinated hamsters. After viral challenge, hamsters were monitored for (A) weight loss, and viral titers were evaluated in (B) nasal turbinates and (C) lung tissues on days 3, 5, and 7 post-infection. *Significantly different from RBD and RBD|Spycage, **significantly different from RBD|SpyCage. Non-parametric Kruskal-Wallis test with Dunn's multiple comparisons were used to determine significant differences.

while viral titers on days 3 and 7 in the nasal turbinates and lungs were comparable for all groups, on day 5 viral titers in the RBD + SpyCage vaccinated animals were more than 10-fold lower, indicating that the RBD + SpyCage vaccinated animals more rapidly cleared SARS-CoV-2 from both the upper and lower respiratory tracts.

Last, we performed a histopathology analysis to determine if the RBD + SpyCage vaccinated animals had reduced lung inflammation and damage. Lung tissue sections were blinded and scored for the extent of lesions, alveolar, bronchial, and blood vessel damage, as well as hemorrhage and type II pneumocyte hyperplasia. These scores were then combined to give a total pathology score. Representative images of lung pathology and inflammation from each group are shown in Fig. 5A. The largest differences in pathology scores were observed in the total pathology score and the extent of lesions (Fig. 5B and C), with additional scores reported in Fig. S4. On day 3, all groups exhibited similar pathology. For the mock vaccinated animals, the total pathology score and extent of lesions peaked on day 5 and then declined on day 7. The RBD + SpyCage vaccinated animals exhibited the lowest total pathology and extent of lesions scores compared to all other groups on both days 5 and 7. Animals receiving SpyCage, RBD, or the SpyCage|RBD admixture had intermediate scores between the mock and SpyCage + RBD groups on day 5 and had pathology scores comparable to mock infected animals on day 7. While the pathology scoring shows a trend toward reduced pathology with the SpyCage + RBD group, this difference was not statistically significant due to the limited number of animals used at each time point. Future studies can leverage these observed effect sizes to establish expanded group sizes to determine if these promising trends are maintained.

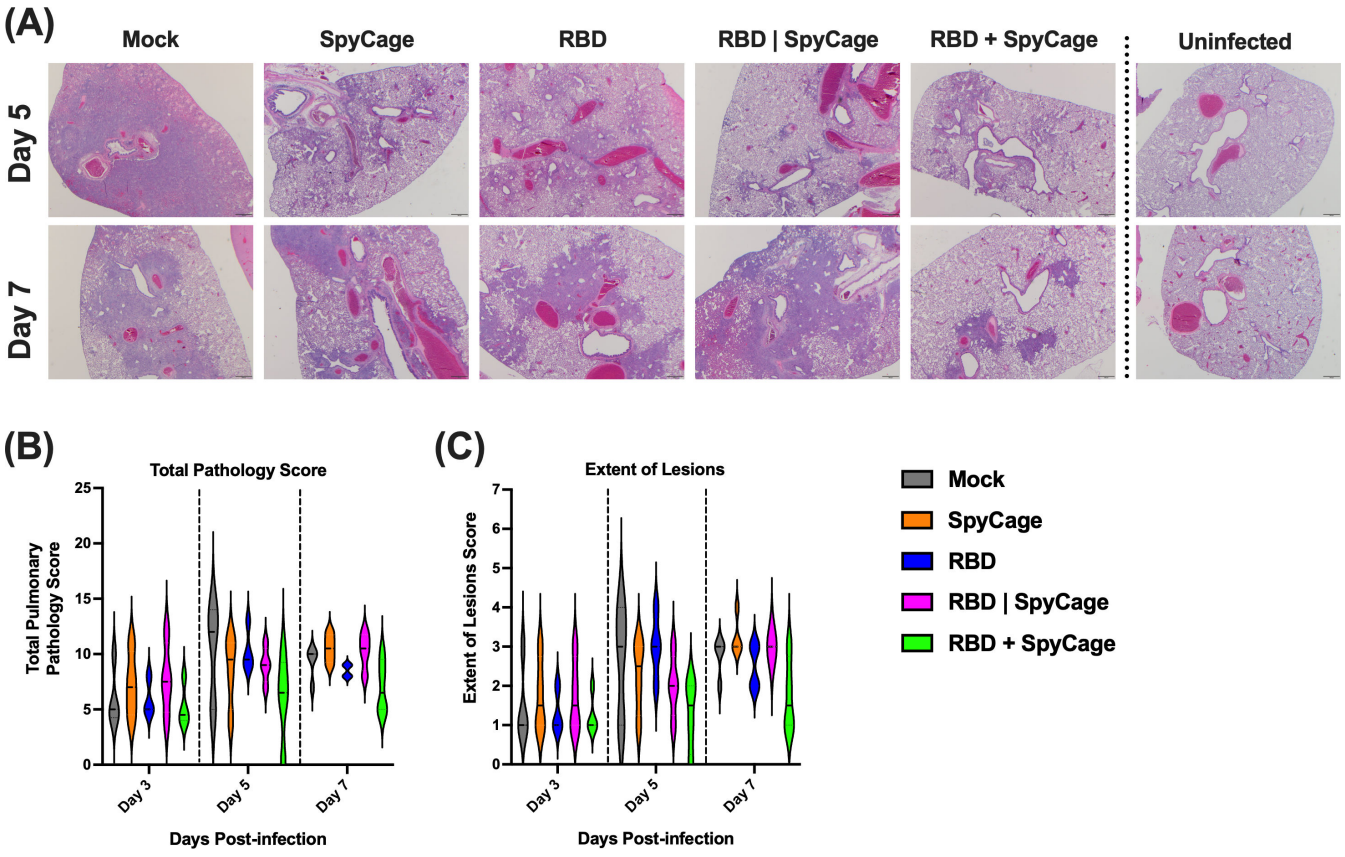

FIG 5 SARS-CoV-2 induced lung pathology in vaccinated hamsters. On days 3, 5, and 7, post-infection, lung tissues were processed for H&E staining and scored by a veterinary pathologist. (A) Representative images from each group of hamsters on days 5 and 7 post-infection. This panel also includes images of uninfected hamster lung tissues (far right panels). Areas of consolidation (dense purple staining) are sites of pathology. (B and C) Total pathology scores and the extent of lesions scoring, respectively.

DISCUSSION

The development of efficacious intranasal vaccines has the potential to prevent SARS-CoV-2 infections and reduce transmission (67). To date, several pre-clinical intranasal vaccine candidates have been developed (18); however, most candidates are live-attenuated or viral vector vaccines. Due to safety concerns, the administration of these vaccines is often limited to healthy adults (18–55 years old) and/or older children. In contrast, recombinant protein or inactivated vaccines are widely used in individuals of all ages. Therefore, we sought to develop a recombinant protein-based intranasal vaccine.

Because immune responses can be enhanced when antigen-of-interest are displayed on a scaffold, we established design criteria for an intranasal vaccine candidate. These criteria included (i) rigid bodies, (ii) a spherical shape of ~20 to 30 nm in diameter, and (iii) genetically accessible N- and C-termini presented in an outward-facing manner. I3-01 met all these criteria and was selected as the strongest candidate. To date, only a lower-resolution cryo-EM reconstruction and a computational model of I3-01 have been published (47). Therefore, we used both negative stain TEM and cryo-EM to resolve the I3-01-based scaffold (apo cage) to a 3.4-Å average resolution and validated that the experimentally derived atomic model closely matched the computationally designed protein (Fig. 1). We then proceeded with using I3-01 to create SpyCage by further modifying I3-01 to bear an N-terminal SpyCatcher domain with a 12-amino acid flexible linker to reduce steric hindrance and permit greater saturation of antigens. As anticipated, the SpyTag/SpyCatcher system enabled rapid, covalent linkage of RBD to SpyCage (RBD + SpyCage) to near saturation as seen by a mobility shift by SDS-PAGE (Fig. 2). Importantly, the RBD + SpyCage preparation remained highly soluble and stable over time, which further supports its feasibility as a vaccine candidate.

Subsequently, we assessed the immunogenicity of the RBD + SpyCage combined with LTA1 as an intranasal adjuvant in the gold standard Syrian hamster model (i.e., trial 1). Animals were given a prime-boost intranasal vaccination 28 days apart and then challenged 28 days later (day 56 post-primary vaccination) with SARS-CoV-2. Immediately prior to challenge (i.e., day 55 post-primary vaccination), four of six and six of six animals in the RBD + SpyCage and RBD + SpyCage + LTA1 groups, respectively, had developed serum IgG antibodies (Fig. S1). In the RBD + SpyCage group, these antibodies did not have neutralizing activity, while in the RBD + SpyCage + LTA1 group, three animals developed low titers of neutralizing antibodies. Following viral challenge, all animals, regardless of vaccination status, lost weight, although there was a trend toward reduced weight loss and earlier recovery in the RBD + SpyCage and RBD + SpyCage + LTA1 vaccinated animals (Fig. S2). Based on these outcomes, we next sought to determine if grafting of the RBD to SpyCage was a requirement for vaccine immunogenicity.

Studies on intramuscular vaccination have shown that presenting viral antigens on the surface of particles enhances the immune presentation and protective efficacy of vaccines (68). Therefore, we expanded upon our initial study and compared RBD + SpyCage (in which RBD is covalently bound to the scaffold) to an RBD|SpyCage admixture lacking this covalent attachment. We did not use the LTA1 adjuvant in these studies because it did not enhance protection in trial 1, and because it enhances immunogenicity, potentially obscuring the evaluation of the requirement for grafting to RBD. Covalent grafting to RBD was shown to be a requirement for immunogenicity, as two of six and five of six animals given RBD + SpyCage developed an IgG response to RBD on days 28 and 55, respectively (Fig. 3). The one animal that exhibited the highest IgG titers on day 28 and day 55 also developed an IgA response, and these antibodies exhibited neutralizing activity. In contrast, animals vaccinated with RBD|SpyCage (i.e., RBD mixed with but not covalently bound to SpyCage) did not develop an antibody response to RBD. Further studies are warranted to optimize the dose of LTA1 and evaluate combinations of intranasal adjuvants to enhance the immunogenicity of RBD + SpyCage to match the neutralizing IgG and IgA response we observed in this one animal.

As a final component of our antibody analyses, we evaluated the response generated against the SpyCage scaffold. All animals that received SpyCage as a component of the vaccine developed antibodies directed toward the scaffold. Our results do not suggest this immunity interfered with the immune response to RBD, as boost vaccination increased the response to RBD. However, in future studies, if immunity against the scaffold interferes with immunogenicity for other vaccine antigens, alternative scaffolds can be evaluated for subsequent intranasal vaccinations (69). Importantly, assessment of the immune response in hamsters is currently hampered by a limited number of species-specific reagents. Reagents to assess mucosal and cellular immunity are lacking. Using our existing protocol, we previously performed ELISA on matched convalescent hamster serum and nasal wash samples (23). While we detected serum IgA antibodies, we could not detect antibodies in the nasal wash (data not shown). Therefore, as new reagents are developed for hamsters, it will be important to expand the immunological assessment of vaccine responses.

Covalent grafting to SpyCage was also a requirement for vaccine efficacy. Upon SARS-CoV-2 challenge in trial 2, all animals lost weight; however, compared to the other groups, RBD + SpyCage vaccinated animals had a trend toward reduced weight loss and reduced lung pathology. This was associated with significantly reduced levels of replicating virus in the respiratory tract on day 5, indicating rapid viral clearance in the RBD + SpyCage group relative to the RBD|SpyCage group (Fig. 4). Future studies could pinpoint a more comprehensive view of the dynamics and changes in viral clearance. Collectively, the induction of non-neutralizing RBD-binding antibodies, in association with accelerated viral clearance and trends toward reduced disease severity and pathology, suggests alternative antibody-mediated mechanisms (e.g., antibody-dependent cell-mediated cytotoxicity or antibody-dependent cellular phagocytosis) and/or that T cell-mediated immunity contributed to protection.

To our knowledge, this is the first report of a scaffolded antigen being used as an intranasal protein-based vaccine. Other groups have used the I3-01 scaffold successfully as a vaccine platform to display antigens for influenza, SARS-CoV-2, and *Plasmodium* but have only explored intramuscular administration (35, 42, 64, 70–73). Several groups have expressed the RBD or S-protein on I3-01 and evaluated the immunogenicity of these scaffolded antigens as intramuscular vaccines in animal models (42, 64, 70–72). In these studies, the vaccine candidates were administered with an adjuvant (e.g., AddaVax, alum, and CpG), and potent neutralizing antibody responses were induced in mice, hamsters, pigs, or non-human primates (42, 64, 70–72). Given both the route of administration and the inclusion of adjuvants, this is the expected antibody response. In comparison, in trials 1 and 2, animals that received the SpyCage + RBD vaccine developed non-neutralizing IgG antibodies. When LTA1 was added to the vaccine in trial 1, all animals developed an IgG response, but only three of six animals developed low titers of neutralizing antibodies.

Prior studies have evaluated the protective efficacy of intramuscular vaccination with RBD grafted to I3-01 against SARS-CoV-2 challenge (42, 64). When hamsters were intramuscularly vaccinated and challenged with SARS-CoV-2, consistent with our results, all animals lost weight, and the RBD-I3-01 vaccinated animals (designated "RBD-VLP" in that study) had reduced weight loss relative to animals vaccinated with RBD alone (42). Unfortunately, in this study, viral titers were not evaluated in lung or nasal turbinate samples after viral infection, precluding a comparison with our findings. In another study, when transgenic K18-hACE2 mice were vaccinated with a similar construct, SARS-CoV-2 Beta RBD-mi3, and challenged, all vaccinated mice survived a lethal challenge, while only 20% of control animals survived. In parallel, with enhanced survival, no replicating virus was detected in the lungs of the RBD-mi3 vaccinated animals (64). Similarly, when Rhesus macaques were vaccinated with the same construct and challenged with SARS-CoV-2, at both days 2 and 4 p.i., significantly lower titers of virus were detected in nasal swabs compared to unimmunized controls. Moreover, in RBD-mi3 vaccinated animals, replicating virus was not recovered from bronchioloalveolar lavage fluids (BAL) (i.e., zero

of four), while three of four unimmunized controls had between 10^3 and 10^6 $TCID_{50}$/mL of SARS-CoV-2 in the BAL (64). In addition to I3-01, the bipartite I53-50 icosahedral scaffold consisting of 120-subunit proteins has also been decorated with either the RBD or S-protein and utilized as an intramuscular vaccine (34, 74). Consistent with intramuscular vaccination with I3-01, intramuscular vaccination with RBD or S-protein grafted to I53-50 combined with an adjuvant induced a neutralizing antibody response in mice, rabbits, or macaques (34, 74). In these studies, only macaques vaccinated with S-protein on I53-50 nanoparticles were challenged with SARS-CoV-2. Following viral challenge, relative to unimmunized controls, vaccinated animals had reduced clinical manifestations associated with significantly reduced viral titers in the upper airways and BAL from day 1 until resolution on day 7 p.i (34). In contrast to these studies, when we challenged the RBD + SpyCage vaccinated animals, we did not observe an initial reduction in SARS-CoV-2 replication as all animals had similar titers on day 3 p.i.; however, the RBD + SpyCage vaccinated animals had reduced titers on day 5, indicating accelerated viral clearance. We also observed trends toward reduced weight loss and reduced pathology; however, these were not statistically significant. The reduced efficacy observed in our studies relative to intramuscular vaccination is most likely due to a lack of a neutralizing antibody response following intranasal vaccination. Indeed, in recent studies, intranasal vaccination of hamsters with bacterial extracellular vesicles decorated with RBD or S protein induced neutralizing antibodies that reduced or prevented viral replication and clinical disease (75, 76). Therefore, future development of the intranasal RBD + SpyCage vaccine warrants further optimization of the LTA1 adjuvant and/or inclusion of additional potential intranasal adjuvants to enhance the quality of the antibody response and vaccine efficacy. In addition, to more closely model immunity in the human population, a recent study explored intranasal vaccination with recombinant S-protein as a booster in animals previously given intramuscular vaccines (77). This approach enhanced protection, and based on our findings, we posit that such an intranasal boost would benefit from scaffolding the S-protein or its derivatives.

Collectively, we demonstrate intranasal vaccination with RBD grafted to SpyCage induced a serum IgG response in hamsters. Upon viral challenge, this response was associated with enhanced viral clearance from both the upper and lower respiratory tracts. RBD + SpyCage vaccinated animals also exhibited non-significant reductions in weight loss and lung pathology consistent with a non-neutralizing antibody response. We further show the immunogenicity and efficacy of the RBD + SpyCage vaccine required that RBD was covalently linked to the SpyCage scaffold. These studies demonstrate the potential for intranasal delivery of SpyCage scaffolded antigens as a vaccine platform, and additional vaccine development is warranted with the inclusion of intranasal adjuvants to enhance immunogenicity. Moreover, given the relative ease with which vaccine antigens can be grafted to the scaffold and the potential to induce mucosal immunity, SpyCage-derived intranasal vaccines can be developed to target other respiratory viruses, and if successful, this platform could also be used as a rapid response vaccine platform to target novel or pandemic pathogens.

ACKNOWLEDGMENTS

S.H., S.E.L., and T.C.S. planned all experiments with assistance from D.R.P. and A.M. A.M. and S.E.L. designed and purified recombinant proteins and vaccine candidates. R.M.R. expressed the RBD protein. E.B.M. provided LTA1 adjuvant and guidance on use of the adjuvant. All cryo-EM studies were conducted by C.B., I.M.M., and S.H. Vaccination and challenge studies were conducted by D.R.P. with assistance from D.G.S., C.J.F., A.K., and T.H. E.H.L. performed histopathology and analysis of lung samples. D.R.P., E.B.N., S.H., S.E.L., and T.C.S. prepared the final manuscript.

The molecular graphics and analyses were performed with UCSF ChimeraX, developed by the Resource for Biocomputing, Visualization, and Informatics at the University of California, San Francisco, with support from National Institutes of Health R01-GM129325 and the Office of Cyber Infrastructure and Computational Biology,

National Institute of Allergy and Infectious Diseases. We acknowledge Dr. David Baker from the University of Washington for providing I3-01_HisR4 plasmid, Dr. Florian Krammer from Mount Sinai School of Medicine, for providing the pCAGGS plasmid for SARS-CoV-2 Spike RBD expression, and Dr. Sabra Klein, Johns Hopkins, School of Public Health, for generously providing the IgG and IgA enzyme-linked immunosorbent assay protocols. We also acknowledge Bob Ashley at Penn State College of Medicine for pilot electron microscopy efforts. Lastly, we would also like to acknowledge the Sartorius Huck Cell Culture Facility for early access and production of SARS-CoV-2 Spike RBD protein (RRID:SCR_024463).

The design and expression of the SpyCage scaffold was conducted by S.E.L. and S.H. under NIGMS R01GM125907. Seed Grant funding to S.E.L. and T.C.S. from the Pennsylvania State University Huck Institutes of Life Sciences supported the vaccination and challenge studies. Funding for T.C.S. was also provided by the US Department of Agriculture National Institute of Food and Agriculture, Hatch project 4771, and The Huck Institutes of Life Sciences.

AUTHOR AFFILIATIONS

[1]Department of Veterinary and Biomedical Sciences, Pennsylvania State University, University Park, Pennsylvania, USA
[2]The Huck Institutes of Life Sciences, Pennsylvania State University, University Park, Pennsylvania, USA
[3]Department of Biochemistry and Molecular Biology, Pennsylvania State University, University Park, Pennsylvania, USA
[4]The Huck Center for Malaria Research, University Park, Pennsylvania, USA
[5]Department of Biology, Pennsylvania State University, University Park, Pennsylvania, USA
[6]Animal Diagnostic Laboratory, Pennsylvania State University, University Park, Pennsylvania, USA
[7]Department of Microbiology and Immunology, Tulane University, New Orleans, Louisiana, USA
[8]Department of Medicine, Pennsylvania State University, University Park, Pennsylvania, USA

PRESENT ADDRESS

Susan L. Hafenstein, The Hornel Institute, University of Minnesota, Austin, Minnesota, USA

AUTHOR ORCIDs

Susan L. Hafenstein http://orcid.org/0000-0003-2609-4036
Scott E. Lindner http://orcid.org/0000-0003-1799-3726
Troy C. Sutton http://orcid.org/0000-0002-7880-4784

FUNDING

Funder	Grant(s)	Author(s)
HHS | NIH | National Institute of General Medical Sciences (NIGMS)	R01GM125907	Susan L. Hafenstein Scott E. Lindner
U.S. Department of Agriculture (USDA)	Hatch Act 4771	Troy C. Sutton
Huck Institutes of Life Science, Pennsylvania State University	Seed Funding	Scott E. Lindner Troy C. Sutton

AUTHOR CONTRIBUTIONS

Devanshi R. Patel, Conceptualization, Formal analysis, Investigation, Methodology, Writing – original draft, Writing – review and editing | Allen M. Minns, Formal analysis, Investigation, Methodology, Resources | Derek G. Sim, Investigation, Methodology | Cassandra J. Field, Formal analysis, Investigation, Methodology, Writing – review and editing | Abigail E. Kerr, Investigation, Methodology | Talia A. Heinly, Investigation, Methodology | Erin H. Luley, Formal analysis, Investigation, Methodology, Writing – review and editing | Randall M. Rossi, Methodology | Carol M. Bator, Data curation, Formal analysis, Methodology, Visualization | Ibrahim M. Moustafa, Data curation, Formal analysis, Investigation, Methodology, Validation, Visualization | Elizabeth B. Norton, Conceptualization, Formal analysis, Resources, Writing – review and editing | Susan L. Hafenstein, Conceptualization, Data curation, Formal analysis, Funding acquisition, Investigation, Methodology, Project administration, Resources, Supervision, Writing – review and editing | Scott E. Lindner, Conceptualization, Data curation, Formal analysis, Funding acquisition, Investigation, Methodology, Project administration, Resources, Supervision, Writing – original draft, Writing – review and editing | Troy C. Sutton, Conceptualization, Data curation, Formal analysis, Funding acquisition, Investigation, Methodology, Project administration, Resources, Supervision, Writing – original draft, Writing – review and editing

DATA AVAILABILITY

The icosahedral map of the solved apo cage structure is deposited in Electron Microscopy Data Bank under accession code EMD-27812. The apo cage atomic model is deposited in the Protein Data Bank under ID 8E01.

ETHICS APPROVAL

All animal studies were conducted in compliance with the Pennsylvania State University Institutional Animal Care and Use Committee under protocol number 202001440.

ADDITIONAL FILES

The following material is available online.

Supplemental Material

Supplemental material (Spectrum04998-22-s0001.pdf). Figures S1 to S4, Table S1, and File S1.

REFERENCES

1. Zhu N, Zhang D, Wang W, Li X, Yang B, Song J, Zhao X, Huang B, Shi W, Lu R, Niu P, Zhan F, Ma X, Wang D, Xu W, Wu G, Gao GF, Tan W, China Novel Coronavirus Investigating and Research Team. 2020. A novel coronavirus from patients with pneumonia in China, 2019. N Engl J Med 382:727–733. https://doi.org/10.1056/NEJMoa2001017
2. Kadam SB, Sukhramani GS, Bishnoi P, Pable AA, Barvkar VT. 2021. SARS - CoV - 2, the pandemic coronavirus: molecular and structural insights. J Basic Microbiol 61:180–202. https://doi.org/10.1002/jobm.202000537
3. Fehr AR, Perlman S. 2015. Coronaviruses, p 1–23. Springer New York.
4. Premkumar L, Segovia-Chumbez B, Jadi R, Martinez DR, Raut R, Markmann A, Cornaby C, Bartelt L, Weiss S, Park Y, Edwards CE, Weimer E, Scherer EM, Rouphael N, Edupuganti S, Weiskopf D, Tse LV, Hou YJ, Margolis D, Sette A, Collins MH, Schmitz J, Baric RS, de Silva AM. 2020. The receptor-binding domain of the viral spike protein is an immunodominant and highly specific target of antibodies in SARS-CoV-2 patients. Sci Immunol 5:eabc8413. https://doi.org/10.1126/sciimmunol.abc8413
5. Piccoli L, Park Y-J, Tortorici MA, Czudnochowski N, Walls AC, Beltramello M, Silacci-Fregni C, Pinto D, Rosen LE, Bowen JE, et al. 2020. Mapping neutralizing and immunodominant sites on the SARS-CoV-2 spike receptor-binding domain by structure-guided high-resolution serology. Cell 183:1024–1042. https://doi.org/10.1016/j.cell.2020.09.037
6. Krammer F. 2020. SARS-CoV-2 vaccines in development. Nature 586:516–527. https://doi.org/10.1038/s41586-020-2798-3
7. World Health Organization. COVID-19 vaccine tracker and landscape
8. COVID-19 vaccines: the full list. 2022. https://covidvax.org.
9. Wu Z, Hu Y, Xu M, Chen Z, Yang W, Jiang Z, Li M, Jin H, Cui G, Chen P, Wang L, Zhao G, Ding Y, Zhao Y, Yin W. 2021. Safety, tolerability, and immunogenicity of an inactivated SARS-CoV-2 vaccine (CoronaVac) in healthy adults aged 60 years and older: a randomised, double-blind, placebo-controlled, phase 1/2 clinical trial. Lancet Infect Dis 21:803–812. https://doi.org/10.1016/S1473-3099(20)30987-7
10. Zhang Y, Zeng G, Pan H, Li C, Hu Y, Chu K, Han W, Chen Z, Tang R, Yin W, Chen X, Hu Y, Liu X, Jiang C, Li J, Yang M, Song Y, Wang X, Gao Q, Zhu F. 2021. Safety, tolerability, and immunogenicity of an inactivated SARS-CoV-2 vaccine in healthy adults aged 18-59 years: a randomised, double-blind, placebo-controlled, phase 1/2 clinical trial. Lancet Infect Dis 21:181–192. https://doi.org/10.1016/S1473-3099(20)30843-4
11. Zakarya K, Kutumbetov L, Orynbayev M, Abduraimov Y, Sultankulova K, Kassenov M, Sarsenbayeva G, Kulmagambetov I, Davlyatshin T, Sergeeva

M, Stukova M, Khairullin B. 2021. Safety and immunogenicity of a QazCovid-in inactivated whole-virion vaccine against COVID-19 in healthy adults: a single-centre, randomised, single-blind, placebo-controlled phase 1 and an open-label phase 2 clinical trials with a 6 months follow-up in Kazakhstan. EClinicalMedicine 39:101078. https://doi.org/10.1016/j.eclinm.2021.101078
12. Xia S, Duan K, Zhang Y, Zhao D, Zhang H, Xie Z, Li X, Peng C, Zhang Y, Zhang W, et al. 2020. Effect of an inactivated vaccine against SARS-CoV-2 on safety and immunogenicity outcomes: interim analysis of 2 randomized clinical trials. JAMA 324:951–960. https://doi.org/10.1001/jama.2020.15543
13. Al Kaabi N, Zhang Y, Xia S, Yang Y, Al Qahtani MM, Abdulrazzaq N, Al Nusair M, Hassany M, Jawad JS, Abdalla J, et al. 2021. Effect of 2 inactivated SARS-CoV-2 vaccines on symptomatic COVID-19 infection in adults: a randomized clinical trial. JAMA 326:35–45. https://doi.org/10.1001/jama.2021.8565
14. Xia X. 2021. Detailed dissection and critical evaluation of the Pfizer/BioNTech and moderna mRNA vaccines. Vaccines (Basel) 9:734. https://doi.org/10.3390/vaccines9070734
15. Creech CB, Walker SC, Samuels RJ. 2021. SARS-CoV-2 vaccines. JAMA 325:1318–1320. https://doi.org/10.1001/jama.2021.3199
16. Machhi J, Shahjin F, Das S, Patel M, Abdelmoaty MM, Cohen JD, Singh PA, Baldi A, Bajwa N, Kumar R, et al. 2021. Nanocarrier vaccines for SARS-CoV-2. Adv Drug Deliv Rev 171:215–239. https://doi.org/10.1016/j.addr.2021.01.002
17. Study of the safety, reactogenicity and immunogenicity of "EpiVacCorona" vaccine for the prevention of COVID-19.2022. ClinicalTrials.gov.
18. Chavda VP, Vora LK, Pandya AK, Patravale VB. 2021. Intranasal vaccines for SARS-CoV-2: from challenges to potential in COVID-19 management. Drug Discov Today 26:2619–2636. https://doi.org/10.1016/j.drudis.2021.07.021
19. Chan JF-W, Zhang AJ, Yuan S, Poon VK-M, Chan CC-S, Lee AC-Y, Chan W-M, Fan Z, Tsoi H-W, Wen L, Liang R, Cao J, Chen Y, Tang K, Luo C, Cai J-P, Kok K-H, Chu H, Chan K-H, Sridhar S, Chen Z, Chen H, To KK-W, Yuen K-Y. 2020. Simulation of the clinical and pathological manifestations of coronavirus disease 2019 (COVID-19) in a golden Syrian hamster model: implications for disease pathogenesis and transmissibility. Clin Infect Dis 71:2428–2446. https://doi.org/10.1093/cid/ciaa325
20. Imai M, Iwatsuki-Horimoto K, Hatta M, Loeber S, Halfmann PJ, Nakajima N, Watanabe T, Ujie M, Takahashi K, Ito M, et al. 2020. Syrian hamsters as a small animal model for SARS-CoV-2 infection and countermeasure development. Proc Natl Acad Sci U S A 117:16587–16595. https://doi.org/10.1073/pnas.2009799117
21. Rosenke K, Meade-White K, Letko M, Clancy C, Hansen F, Liu Y, Okumura A, Tang-Huau T-L, Li R, Saturday G, Feldmann F, Scott D, Wang Z, Munster V, Jarvis MA, Feldmann H. 2020. Defining the Syrian hamster as a highly susceptible preclinical model for SARS-CoV-2 infection. Emerg Microbes Infect 9:2673–2684. https://doi.org/10.1080/22221751.2020.1858177
22. Sia SF, Yan L-M, Chin AWH, Fung K, Choy K-T, Wong AYL, Kaewpreedee P, Perera RAPM, Poon LLM, Nicholls JM, Peiris M, Yen H-L. 2020. Pathogenesis and transmission of SARS-CoV-2 in golden hamsters. Nature 583:834–838. https://doi.org/10.1038/s41586-020-2342-5
23. Field CJ, Heinly TA, Patel DR, Sim DG, Luley E, Gupta SL, Vanderford TH, Wrammert J, Sutton TC. 2022. Immune durability and protection against SARS-CoV-2 re-infection in Syrian hamsters. Emerg Microbes Infect 11:1103–1114. https://doi.org/10.1080/22221751.2022.2058419
24. Yusuf H, Kett V. 2017. Current prospects and future challenges for nasal vaccine delivery. Hum Vaccin Immunother 13:34–45. https://doi.org/10.1080/21645515.2016.1239668
25. Chemaitelly H, Tang P, Hasan MR, AlMukdad S, Yassine HM, Benslimane FM, Al Khatib HA, Coyle P, Ayoub HH, Al Kanaani Z, Al Kuwari E, Jeremijenko A, Kaleeckal AH, Latif AN, Shaik RM, Abdul Rahim HF, Nasrallah GK, Al Kuwari MG, Al Romaihi HE, Butt AA, Al-Thani MH, Al Khal A, Bertollini R, Abu-Raddad LJ. 2021. Waning of BNT162b2 vaccine protection against SARS-CoV-2 infection in Qatar. N Engl J Med 385:e83. https://doi.org/10.1056/NEJMoa2114114
26. Keehner J, Horton LE, Binkin NJ, Laurent LC, Pride D, Longhurst CA, Abeles SR, Torriani FJ, SEARCH Alliance. 2021. Resurgence of SARS-CoV-2 infection in a highly vaccinated health system workforce. N Engl J Med 385:1330–1332. https://doi.org/10.1056/NEJMc2112981
27. Chan RWY, Liu S, Cheung JY, Tsun JGS, Chan KC, Chan KYY, Fung GPG, Li AM, Lam HS. 2021. The mucosal and serological immune responses to the novel coronavirus (SARS-CoV-2) vaccines. Front Immunol 12:744887. https://doi.org/10.3389/fimmu.2021.744887
28. Hajnik RL, Plante JA, Liang Y, Alameh M-G, Tang J, Bonam SR, Zhong C, Adam A, Scharton D, Rafael GH, Liu Y, Hazell NC, Sun J, Soong L, Shi P-Y, Wang T, Walker DH, Sun J, Weissman D, Weaver SC, Plante KS, Hu H. 2022. Dual spike and nucleocapsid mRNA vaccination confer protection against SARS-CoV-2 omicron and delta variants in preclinical models. Sci Transl Med 14:eabq1945. https://doi.org/10.1126/scitranslmed.abq1945
29. Lund FE, Randall TD. 2021. Scent of a vaccine. Science 373:397–399. https://doi.org/10.1126/science.abg9857
30. Topol EJ, Iwasaki A. 2022. Operation nasal vaccine-lightning speed to counter COVID-19. Sci Immunol 7:eadd9947. https://doi.org/10.1126/sciimmunol.add9947
31. WHO. 2022. The Oxford/AstraZeneca (ChAdOx1-S [recombinant] vaccine) COVID-19 vaccine: what you need to know. Available from: https://www.who.int/news-room/feature-stories/detail/the-oxford-astrazeneca-covid-19-vaccine-what-you-need-to-know
32. U.S. Food and Drug Administration. 2022. Coronavirus (COVID-19) update: FDA limits use of Janssen COVID-19 vaccine to certain individuals. Available from: https://www.fda.gov/news-events/press-announcements/coronavirus-covid-19-update-fda-limits-use-janssen-covid-19-vaccine-certain-individuals
33. Sridhar S, Brokstad KA, Cox RJ. 2015. Influenza vaccination strategies: comparing inactivated and live attenuated influenza vaccines. Vaccines (Basel) 3:373–389. https://doi.org/10.3390/vaccines3020373
34. Brouwer PJM, Brinkkemper M, Maisonnasse P, Dereuddre-Bosquet N, Grobben M, Claireaux M, de Gast M, Marlin R, Chesnais V, Diry S, et al. 2021. Two-component spike nanoparticle vaccine protects macaques from SARS-CoV-2 infection. Cell 184:1188–1200. https://doi.org/10.1016/j.cell.2021.01.035
35. Bruun TUJ, Andersson A-MC, Draper SJ, Howarth M. 2018. Engineering a rugged nanoscaffold to enhance plug-and-display vaccination. ACS Nano 12:8855–8866. https://doi.org/10.1021/acsnano.8b02805
36. Caradonna TM, Schmidt AG. 2021. Protein engineering strategies for rational immunogen design. NPJ Vaccines 6:154. https://doi.org/10.1038/s41541-021-00417-1
37. Cohen AA, Gnanapragasam PNP, Lee YE, Hoffman PR, Ou S, Kakutani LM, Keeffe JR, Wu H-J, Howarth M, West AP, Barnes CO, Nussenzweig MC, Bjorkman PJ. 2021. Mosaic nanoparticles elicit cross-reactive immune responses to zoonotic coronaviruses in mice. Science 371:735–741. https://doi.org/10.1126/science.abf6840
38. Hsieh CL, McLellan JS. 2022. Protein engineering responses to the COVID-19 pandemic. Curr Opin Struct Biol 74:102385. https://doi.org/10.1016/j.sbi.2022.102385
39. Liu Z-H, Xu H-L, Han G-W, Tao L-N, Lu Y, Zheng S-Y, Fang W-H, He F. 2021. Self-assembling nanovaccine enhances protective efficacy against CSFV in pigs. Front Immunol 12:689187. https://doi.org/10.3389/fimmu.2021.689187
40. Malhi H, Homad LJ, Wan Y-H, Poudel B, Fiala B, Borst AJ, Wang JY, Walkey C, Price J, Wall A, Singh S, Moodie Z, Carter L, Handa S, Correnti CE, Stoddard BL, Veesler D, Pancera M, Olson J, King NP, McGuire AT. 2022. Immunization with a self-assembling nanoparticle vaccine displaying EBV gH/gL protects humanized mice against lethal viral challenge. Cell Rep Med 3:100658. https://doi.org/10.1016/j.xcrm.2022.100658
41. Nguyen B, Tolia NH. 2021. Protein-based antigen presentation platforms for nanoparticle vaccines. NPJ Vaccines 6:70. https://doi.org/10.1038/s41541-021-00330-7
42. Dalvie NC, Rodriguez-Aponte SA, Hartwell BL, Tostanoski LH, Biedermann AM, Crowell LE, Kaur K, Kumru OS, Carter L, Yu J, et al. 2021. Engineered SARS-CoV-2 receptor binding domain improves manufacturability in yeast and immunogenicity in mice. Proc Natl Acad Sci U S A 118:e2106845118. https://doi.org/10.1073/pnas.2106845118
43. Iwanaga N, Chen K, Yang H, Lu S, Hoffmann JP, Wanek A, McCombs JE, Song K, Rangel-Moreno J, Norton EB, Kolls JK. 2021. Vaccine-driven lung TRM cells provide immunity against *Klebsiella* via fibroblast IL-17R signaling. Sci Immunol 6:eabf1198. https://doi.org/10.1126/sciimmunol.abf1198
44. Norton EB, Lawson LB, Mahdi Z, Freytag LC, Clements JD. 2012. The A subunit of *Escherichia coli* heat-labile enterotoxin functions as a mucosal

adjuvant and promotes IgG2a, IgA, and Th17 responses to vaccine antigens. Infect Immun 80:2426–2435. https://doi.org/10.1128/IAI.00181-12
45. Valli E, Baudier RL, Harriett AJ, Norton EB. 2020. LTA1 and dmLT enterotoxin-based proteins activate antigen-presenting cells independent of PKA and despite distinct cell entry mechanisms. PLoS One 15:e0227047. https://doi.org/10.1371/journal.pone.0227047
46. Valli E, Harriett AJ, Nowakowska MK, Baudier RL, Provosty WB, McSween Z, Lawson LB, Nakanishi Y, Norton EB. 2019. LTA1 is a safe, intranasal enterotoxin-based adjuvant that improves vaccine protection against influenza in young, old and B-cell-depleted (muMT) mice. Sci Rep 9:15128. https://doi.org/10.1038/s41598-019-51356-w
47. Hsia Y, Bale JB, Gonen S, Shi D, Sheffler W, Fong KK, Nattermann U, Xu C, Huang P-S, Ravichandran R, Yi S, Davis TN, Gonen T, King NP, Baker D. 2016. Design of a hyperstable 60-subunit protein dodecahedron. Nature 535:136–139. https://doi.org/10.1038/nature18010
48. Hsia Y, Bale JB, Gonen S, Shi D, Sheffler W, Fong KK, Nattermann U, Xu C, Huang P-S, Ravichandran R, Yi S, Davis TN, Gonen T, King NP, Baker D. 2016. Corrigendum: design of a hyperstable 60-subunit protein icosahedron. Nature 540:150. https://doi.org/10.1038/nature20108
49. Zakeri B, Fierer JO, Celik E, Chittock EC, Schwarz-Linek U, Moy VT, Howarth M. 2012. Peptide tag forming a rapid covalent bond to a protein, through engineering a bacterial adhesin. Proc Natl Acad Sci U S A 109:E690–7. https://doi.org/10.1073/pnas.1115485109
50. Punjani A, Rubinstein JL, Fleet DJ, Brubaker MA. 2017. cryoSPARC: algorithms for rapid unsupervised cryo-EM structure determination. Nat Methods 14:290–296. https://doi.org/10.1038/nmeth.4169
51. Bepler T, Morin A, Rapp M, Brasch J, Shapiro L, Noble AJ, Berger B. 2019. Positive-unlabeled convolutional neural networks for particle picking in cryo-electron micrographs. Nat Methods 16:1153–1160. https://doi.org/10.1038/s41592-019-0575-8
52. Rubinstein JL, Brubaker MA. 2015. Alignment of cryo-EM movies of individual particles by optimization of image translations. J Struct Biol 192:188–195. https://doi.org/10.1016/j.jsb.2015.08.007
53. Pettersen EF, Goddard TD, Huang CC, Meng EC, Couch GS, Croll TI, Morris JH, Ferrin TE. 2021. UCSF ChimeraX: structure visualization for researchers, educators, and developers. Protein Sci 30:70–82. https://doi.org/10.1002/pro.3943
54. Liebschner D, Afonine PV, Baker ML, Bunkóczi G, Chen VB, Croll TI, Hintze B, Hung LW, Jain S, McCoy AJ, Moriarty NW, Oeffner RD, Poon BK, Prisant MG, Read RJ, Richardson JS, Richardson DC, Sammito MD, Sobolev OV, Stockwell DH, Terwilliger TC, Urzhumtsev AG, Videau LL, Williams CJ, Adams PD. 2019. Macromolecular structure determination using X-rays, neutrons and electrons: recent developments in Phenix. Acta Crystallogr D Struct Biol 75:861–877. https://doi.org/10.1107/S2059798319011471
55. Emsley P, Lohkamp B, Scott WG, Cowtan K. 2010. Features and development of *Coot*. Acta Crystallogr D Biol Crystallogr 66:486–501. https://doi.org/10.1107/S0907444910007493
56. Williams CJ, Headd JJ, Moriarty NW, Prisant MG, Videau LL, Deis LN, Verma V, Keedy DA, Hintze BJ, Chen VB, Jain S, Lewis SM, Arendall WB 3rd, Snoeyink J, Adams PD, Lovell SC, Richardson JS, Richardson DC. 2018. MolProbity: more and better reference data for improved all-atom structure validation. Protein Sci 27:293–315. https://doi.org/10.1002/pro.3330
57. Reed LJ, Muench H. 1938. A simple method of estimating fifty per cent endpoints12. Am J Epidemiol. 27:493–497. https://doi.org/10.1093/oxfordjournals.aje.a118408
58. Sutton TC, Lamirande EW, Czako R, Subbarao K. 2017. Evaluation of the biological properties and cross-reactive antibody response to H10 influenza viruses in ferrets. J Virol 91:e00895-17. https://doi.org/10.1128/JVI.00895-17
59. Patel DR, Field CJ, Septer KM, Sim DG, Jones MJ, Heinly TA, Vanderford TH, McGraw EA, Sutton TC, Gallagher T. 2021. Transmission and protection against reinfection in the ferret model with the SARS-CoV-2 USA-WA1/2020 reference isolate. J Virol 95:e0223220. https://doi.org/10.1128/JVI.02232-20
60. Dhakal S, Ruiz-Bedoya CA, Zhou R, Creisher PS, Villano JS, Littlefield K, Ruelas Castillo J, Marinho P, Jedlicka AE, Ordonez AA, et al. 2021. Sex differences in lung imaging and SARS-CoV-2 antibody responses in a COVID-19 golden Syrian hamster model. mBio 12:e0097421. https://doi.org/10.1128/mBio.00974-21
61. Gerhards NM, Cornelissen JBWJ, van Keulen LJM, Harders-Westerveen J, Vloet R, Smid B, Vastenhouw S, van Oort S, Hakze-van der Honing RW, Gonzales JL, Stockhofe-Zurwieden N, de Jong R, van der Poel WHM, Vreman S, Kortekaas J, Wichgers Schreur PJ, Oreshkova N. 2021. Predictive value of precision-cut lung slices for the susceptibility of three animal species for SARS-CoV-2 and validation in a refined hamster model. Pathogens 10:824. https://doi.org/10.3390/pathogens10070824
62. Rosenthal PB, Henderson R. 2003. Optimal determination of particle orientation, absolute hand, and contrast loss in single-particle electron cryomicroscopy. J Mol Biol 333:721–745. https://doi.org/10.1016/j.jmb.2003.07.013
63. Prisant MG, Williams CJ, Chen VB, Richardson JS, Richardson DC. 2020. New tools in MolProbity validation: CaBLAM for CryoEM backbone, UnDowser to rethink "waters," and NGL viewer to recapture online 3D graphics. Protein Sci 29:315–329. https://doi.org/10.1002/pro.3786
64. Cohen AA, van Doremalen N, Greaney AJ, Andersen H, Sharma A, Starr TN, Keeffe JR, Fan C, Schulz JE, Gnanapragasam PNP, Kakutani LM, West AP, Saturday G, Lee YE, Gao H, Jette CA, Lewis MG, Tan TK, Townsend AR, Bloom JD, Munster VJ, Bjorkman PJ. 2022. Mosaic RBD nanoparticles protect against challenge by diverse sarbecoviruses in animal models. Science 377:eabq0839. https://doi.org/10.1126/science.abq0839
65. Karimzadeh S, Bhopal R, Nguyen Tien H. 2021. Review of infective dose, routes of transmission and outcome of COVID-19 caused by the SARS-COV-2: comparison with other respiratory viruses. Epidemiol Infect 149:e96. https://doi.org/10.1017/S0950268821000790
66. Prentiss M, Chu A, Berggren KK. 2022. Finding the infectious dose for COVID-19 by applying an airborne-transmission model to superspreader events. PLoS One 17:e0265816. https://doi.org/10.1371/journal.pone.0265816
67. Focosi D, Maggi F, Casadevall A. 2022. Mucosal vaccines, sterilizing immunity, and the future of SARS-CoV-2 virulence. Viruses 14:187. https://doi.org/10.3390/v14020187
68. Bachmann MF, Jennings GT. 2010. Vaccine delivery: a matter of size, geometry, kinetics and molecular patterns. Nat Rev Immunol 10:787–796. https://doi.org/10.1038/nri2868
69. Ueda G, Antanasijevic A, Fallas JA, Sheffler W, Copps J, Ellis D, Hutchinson GB, Moyer A, Yasmeen A, Tsybovsky Y, et al. 2020. Tailored design of protein nanoparticle scaffolds for multivalent presentation of viral glycoprotein antigens. Elife 9:e57659. https://doi.org/10.7554/eLife.57659
70. He L, Lin X, Wang Y, Abraham C, Sou C, Ngo T, Zhang Y, Wilson IA, Zhu J. 2021. Single-component, self-assembling, protein nanoparticles presenting the receptor binding domain and stabilized spike as SARS-CoV-2 vaccine candidates. Sci Adv 7:eabf1591. https://doi.org/10.1126/sciadv.abf1591
71. Kang Y-F, Sun C, Zhuang Z, Yuan R-Y, Zheng Q, Li J-P, Zhou P-P, Chen X-C, Liu Z, Zhang X, Yu X-H, Kong X-W, Zhu Q-Y, Zhong Q, Xu M, Zhong N-S, Zeng Y-X, Feng G-K, Ke C, Zhao J-C, Zeng M-S. 2021. Rapid development of SARS-CoV-2 spike protein receptor-binding domain self-assembled nanoparticle vaccine candidates. ACS Nano 15:2738–2752. https://doi.org/10.1021/acsnano.0c08379
72. Tan TK, Rijal P, Rahikainen R, Keeble AH, Schimanski L, Hussain S, Harvey R, Hayes JWP, Edwards JC, McLean RK, et al. 2021. A COVID-19 vaccine candidate using SpyCatcher multimerization of the SARS-CoV-2 spike protein receptor-binding domain induces potent neutralising antibody responses. Nat Commun 12:542. https://doi.org/10.1038/s41467-020-20654-7
73. Cohen AA, Yang Z, Gnanapragasam PNP, Ou S, Dam K-MA, Wang H, Bjorkman PJ. 2021. Construction, characterization, and immunization of nanoparticles that display a diverse array of influenza HA trimers. PLoS One 16:e0247963. https://doi.org/10.1371/journal.pone.0247963
74. Walls AC, Fiala B, Schäfer A, Wrenn S, Pham MN, Murphy M, Tse LV, Shehata L, O'Connor MA, Chen C, et al. 2020. Elicitation of potent neutralizing antibody responses by designed protein nanoparticle vaccines for SARS-CoV-2. Cell 183:1367–1382. https://doi.org/10.1016/j.cell.2020.10.043
75. Jiang L, Driedonks TAP, Jong WSP, Dhakal S, Bart van den Berg van Saparoea H, Sitaras I, Zhou R, Caputo C, Littlefield K, Lowman M, Chen M, Lima G, Gololobova O, Smith B, Mahairaki V, Riley Richardson M, Mulka KR, Lane AP, Klein SL, Pekosz A, Brayton C, Mankowski JL, Luirink J, Villano JS, Witwer KW. 2022. A bacterial extracellular vesicle-based

intranasal vaccine against SARS-CoV-2 protects against disease and elicits neutralizing antibodies to wild-type and Delta variants. J Extracell Vesicles 11:e12192. https://doi.org/10.1002/jev2.12192
76. van der Ley PA, Zariri A, van Riet E, Oosterhoff D, Kruiswijk CP. 2021. An intranasal OMV-based vaccine induces high mucosal and systemic protecting immunity against a SARS-CoV-2 infection. Front Immunol 12:781280. https://doi.org/10.3389/fimmu.2021.781280
77. Mao T, Israelow B, Peña-Hernández MA, Suberi A, Zhou L, Luyten S, Reschke M, Dong H, Homer RJ, Saltzman WM, Iwasaki A. 2022. Unadjuvanted intranasal spike vaccine elicits protective mucosal immunity against sarbecoviruses. Science 378:eabo2523. https://doi.org/10.1126/science.abo2523